# An Ultrasonically Enhanced Inclined Settler for Microalgae Harvesting

**Esteban Hincapié Gómez and Anthony J. Marchese**
Dept. of Mechanical Engineering, Colorado State University, Fort Collins, CO 80523

*DOI 10.1002/btpr.2031*
*Published online 00 Month 2014 in Wiley Online Library (wileyonlinelibrary.com)*

*Microalgae have vast potential as a sustainable and scalable source of biofuels and bioproducts. However, algae dewatering is a critical challenge that must be addressed. Ultrasonic settling has already been exploited for concentrating various biological cells at relatively small batch volumes and/or low throughput. Typically, these designs are operated in batch or semicontinuous mode, wherein the flow is interrupted and the cells are subsequently harvested. These batch techniques are not well suited for scaleup to the throughput levels required for harvesting microalgae from the large-scale cultivation operations necessary for a viable algal biofuel industry. This article introduces a novel device for the acoustic harvesting of microalgae. The design is based on the coupling of the acoustophoretic force, acoustic transparent materials, and inclined settling. A filtration efficiency of 70 ± 5% and a concentration factor of 11.6 ± 2.2 were achieved at a flow rate of 25 mL·min$^{-1}$ and an energy consumption of 3.6 ± 0.9 kWh·m$^{-3}$. The effects of the applied power, flow rate, inlet cell concentration, and inclination were explored. It was found that the filtration efficiency of the device is proportional to the power applied. However, the filtration efficiency experienced a plateau at 100 W L$^{-1}$ of power density applied. The filtration efficiency also increased with increasing inlet cell concentration and was inversely proportional to the flow rate. It was also found that the optimum settling angle for maximum concentration factor occurred at an angle of 50 ± 5°. At these optimum conditions, the device had higher filtration efficiency in comparison to other similar devices reported in the previous literature.* © 2014 American Institute of Chemical Engineers *Biotechnol. Prog*, 000:000–000, 2014
*Keywords: microalgae, harvesting, dewatering, acoustophoresis, ultrasonic standing waves*

## Introduction

Although numerous technical and environmental challenges must be overcome to realize an economically viable algal biofuel industry, phototrophic microalgae are arguably the only biofuel feedstock that has the productivity required for production at a scale commensurate with global liquid fuel needs. If implemented sustainably into the global energy and food portfolio, microalgal products can reduce greenhouse gas emissions while simultaneously displacing a substantial percentage of our declining fossil fuel resources.[1] Microalgal feedstocks have several potential advantages when compared with current energy crops such as maize, sugarcane, and soybeans. These potential advantages include:

1. *Substantially higher productivity*. Microalgae oil yield is between 10 and 100 times higher (gallons·acre$^{-1}$·year$^{-1}$) when compared with traditional oil crops. Thus microalgae could be the only feedstock with the potential to displace world oil consumption.[2]
2. *No direct competition with food production and the ability to grow in salt water*. Some microalgae strains are able to grow in sea water, which accounts for 70% of the surface area of earth. Furthermore, microalgae could potentially be cultivated in arid land using brackish water.[3]
3. *Potential for carbon dioxide mitigation*. Microalgae consume carbon dioxide at a ratio of 1.83 kg of $CO_2$ per kilogram of biomass. Therefore, microalgal farms could be colocated with power plants as a means of recycling greenhouse $CO_2$.[4]
4. *Coproduction of animal feed*. Microalgae can accumulate up to 54% of dry weight as protein with a similar amino acid profile to the Food and Agricultural Organization reference case for conventional foods.[5]

Despite the potential advantages described above, many challenges must be overcome if microalgae-derived fuels are used to achieve the scale required to displace a substantial percentage of fossil fuels. For example, two critical steps remain that are capital intensive and energy inefficient: the current cost of cultivation at scale and the need for expensive high-speed centrifuges to harvest microalgae.[6] Algae dewatering, in particular, is a critical challenge that must be addressed. As algae are typically cultivated at highly diluted concentrations (approx., 99.9% water), algae dewatering typically represents the most substantial energy sink in the entire microalgae to biofuel value chain.[7] Although gravity settling is an exception in terms of energy requirements, it often requires long residence times or the use of flocculants that could impact downstream processes and/or require substantial operating costs.[8]

Acoustophoresis has been used as the prime force for the separation of different particles and substances such as red blood cells,[9] hybridoma cells,[10] Chinese hamster ovary

Correspondence concerning this article should be addressed to: E. Hincapié Gómez at estebanh@colostate.edu

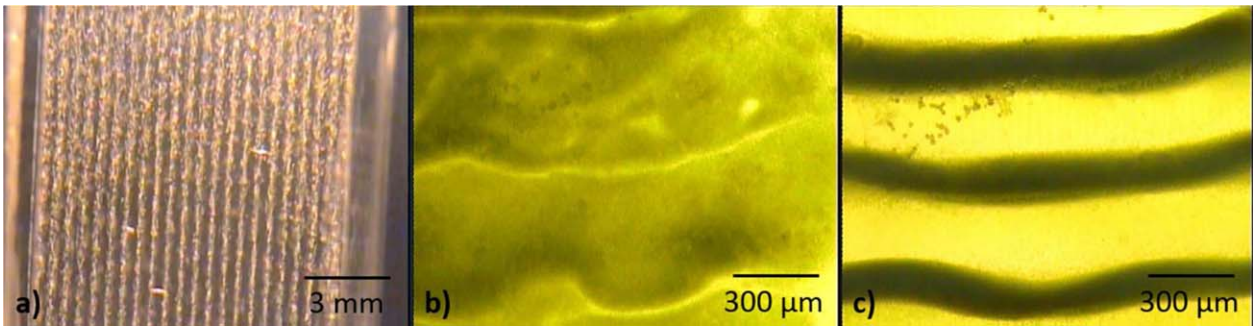


**Figure 1. (a) Laboratory-scale experiment indicating the formation of acoustic agglomeration lines with a 1.7-MHz standing wave in a quartz cuvette using polyamide particles (b) at time = 0 s for the algae strain *N. salina* (c) at $t = 3$ s after applying the acoustic field.**

cells,[11] oil and water emulsions,[12] milk,[13] and palm oil.[14] The acoustophoretic force is gentle and does not affect the viability of the cell.[15] Ultrasonically enhanced sedimentation (UES) is the use of particle agglomeration by acoustophoresis which causes increased gravitational force from larger effective particle size to increase the settling velocity of the low-density cells.[16] Although several acoustic separation devices have been proposed in the prior art, very few of them have been implemented for the separation of microalgae. Most of the current applications in ultrasonic separation are tailored for the production of therapeutic proteins by perfusion filters in bioreactors. A recent thorough review of the state of the art of acoustophoretic separation found only one application for microalgae harvesting by UES.[17] In that study, the authors used a semicontinuous upward flow chamber to harvest the strain *Monodus subterraneus*.[18] In this research, we present the development of a novel acoustic separation device tailored for small, high-lipid content algae cells such as the genus *Nannochloropsis*. The device could also be potentially used for other types of microorganisms such as yeast and mammalian cells.

## Materials and Methods

### *Ultrasonically enhanced sedimentation*

The use of ultrasonic standing waves has been reported in the literature as an approach to manipulate the particles in a fluid. The standing wave is the condition when $f_n = nc/2L$, which is also known as the resonance mode where $f_n$ are the resonance frequencies, $n$ the resonance number, $c$ the speed of sound in the acoustic layer, and $L$ the thickness of the layer. The standing waves exert an acoustic radiation force that agglomerates the particles in acoustic nodes or antinodes. This force moves the cells from the antinodes toward the nodes according to the following equation:[19]

$$F_{ac} = 4\pi R^3 k E_{ac} F \sin 2kx \tag{1}$$

where $R$ is the particle radius ($\mu m^{-1}$), $k$ is the wave number ($m^{-1}$), $E_{ac}$ is the acoustic energy density ($J \cdot m^{-3}$), and $F$ is the acoustic contrast factor. Equation (1) shows that the wavelength of the acoustophoretic force is half that of the acoustic wavelength. Therefore, the acoustophoretic force has alternating bands of zero and its maximum magnitude for every $\lambda/4$ where $\lambda$ is the acoustic wavelength. Also, the acoustic contrast factor, $F$, is an important physical property that has a direct influence on the magnitude of the acoustic force imparted on the particle. The acoustic contrast factor, $F$, can be expressed as follows:[19]

$$F = \frac{1}{3}\left[\frac{5\Lambda - 2}{1 + 2\Lambda} - \frac{1}{\sigma^2 \Lambda}\right] \tag{2}$$

where $\Lambda$ is the ratio of density of particle and the media ($\Lambda = \rho_p/\rho_m$) and $\sigma$ the ratio of the speed of sound in the particle and in the media ($\sigma = c_p/c_m$). The acoustic contrast factor will be different from zero if there is a relative difference in the speed of sound and density between the cell and the surrounding fluid medium. A laboratory scale test performed by our research group is shown in Figure 1 in which the acoustophoretic effect is demonstrated in batch mode using polyamide particles and *N. oculata* cells, respectively. There is, however, a decrease in the acoustophoretic force when $f_n \neq nc/2L$, a condition also known as a progressive wave. For a progressive wave, the acoustophoretic force is much smaller as it is proportional to $R^6$ rather than $R^3$.[20]

The dewatering process of cells by acoustophoresis in an upward flow chamber is a competing effect between different forces. The acoustic and gravity forces act as main drivers for the separation, whereas the drag force associated with the upward fluid velocity has an opposing effect. In the previous study, the use of "pulsed" or "on/off" acoustic cycles, also known as semicontinuous devices, has been suggested as a solution to the drag force problem.[17] Another option suggested in the literature is the use of the displacement of individual cells in the acoustic field, also known as subwavelength design.[17] Although the movement of cells is the primary effect of the acoustophoretic force, this movement is in the order of microns because the frequencies used for this behavior are typically between 1 and 10 MHz[21] and therefore $\lambda/4 = 374$–$37$ µm. Therefore, although this principle has been successfully applied for *Lab-on-Chip* applications, it has not been demonstrated for the large bulk separation required in the bioenergy industry.

Another approach is the use of a continuous flow-enhanced gravity settling as presented below. Assuming the Stokes-derived drag equation for low Reynolds number ($Re < 1$), and the gravity force equation of a particle *suspended* in a fluid, the following equation for critical particle radius can be derived:[22]

$$r_c = \left[\frac{9}{2}\frac{\eta v_f \sin(\gamma)}{(\rho_p - \rho_m) g}\right]^{0.5} \tag{3}$$

Here, the critical particle radius ($r_c$) is the radius at which drag force balances the gravity force (µm), $\eta$ the viscosity of the media ($Pa \cdot s^{-1}$), $v_f$ the fluid velocity ($m \cdot s^{-1}$), $\gamma$ the inclination angle from horizontal axis (°) which is 0° for horizontal flow and 90° for upward flow, $g$ the acceleration owing

to gravity ($m \cdot s^{-2}$), $\rho_p$ the density of the particle ($kg \cdot m^{-3}$), and $\rho_m$ the density of the media ($kg \cdot m^{-3}$). For example, assuming a liquid velocity of 1 $mm \cdot s^{-1}$, the viscosity of water, a vertical orientation with $\gamma = 90°$, a density difference of $\rho_p - \rho_m = 50$ $kg \cdot m^{-3}$, the critical radius is 100 μm, which is roughly equivalent to an agglomerated radius of $3 \times 10^5$ cells. The maximum achievable radius is limited by the frequency of the acoustic wave. The acoustophoretic force will agglomerate the cells in the vicinity of $\lambda/4$ or a maximum agglomerated radius of $\lambda/8$ as it has been explained previously in the literature.[22] Therefore, lower frequencies are better to enhance settling as they create larger clumps. However, it is also important to note that the acoustophoretic force is proportional to the frequency and it is desired to operate at the highest frequency without decreasing the agglomerated radius. Here, the highest frequency to achieve an agglomerated radius of $\lambda/8 = 100$ μm was found to be 1.86 MHz.

A major challenge in utilizing acoustophoretic force for microalgae harvesting is that microalgae cells typically have a density and speed of sound close to the media, which results in very small acoustic contrast factors and hence very low magnitudes of acoustophoretic force ($\boldsymbol{F_{ac}} = 1 \times 10^{-14}$ N). In addition to the problem of low acoustic contrast factor for microalgae cells in water, the small radii of microalgae cells also result in low acoustophoretic force as the force is proportional to the particle radius to the third power. At the same time, the small difference between $\rho_p$ and $\rho_m$ results in a larger critical settling radius, $\boldsymbol{r_c}$, for microalgae ($\boldsymbol{r_c} = 59$ μm and $\rho_p = 1.05$ $g \cdot cm^{-3}$) at a fluid velocity of 0.4 $mm \cdot s^{-1}$ in comparison to other cells such as insect cells ($\boldsymbol{r_c} = 35$ μm and $\rho_p = 1.15$), yeast ($\boldsymbol{r_c} = 41$ μm and $\rho_p = 1.11$) or bacteria ($\boldsymbol{r_c} = 45$ μm and $\rho_p = 1.09$).[18] These factors make microalgae a particularly challenging cell culture to separate by acoustophoresis.

### *Inclined plate settling*

Inclined plate settlers have been widely employed as a separation principle in the wastewater, mineral, and biotechnology industries. In these applications, the media inside the settling chamber precipitate on the inclined plane, creating a sludge layer that slides to the bottom of the container. This principle of settling stratification is also known as the Boycott effect and was originally discovered in an experiment with red blood cells.[23] Inclined settlers have a higher settling area in a smaller footprint when compared with traditional settling devices, which is the reason why they are often called supersettlers. The literature reports successful applications of inclined plate settlers for hybridoma[24] and Chinese hamster ovary cells.[25] However, these applications have been shown to perform well for cells with a mean diameter of between 10 and 20 μm, whereas some algae cells of interest such as *Nannochloropsis* have mean cell diameters of <5 μm.

In this research, the authors suggest a new approach to this challenge, which is the use of an inclined plate in conjunction with ultrasonic standing waves. The ultrasonically enhanced inclined settler (UEIS) device produces acoustic flocculation combined with the compacted area maximization provided by the inclined settler (Figure 2). The main characteristics of the UEIS device are the acoustic chambers with an internal acoustic transparent layer (ATL). The inclined ATL and reflector plate increase the settling area, creating a layered separation of the material as indicated by regions

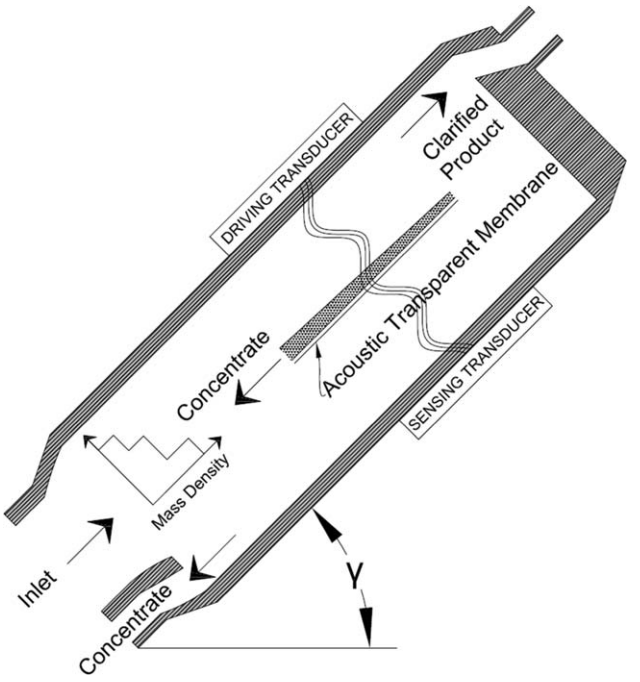


**Figure 2. Schematic diagram of the UEIS device indicating the inclined chamber and ATL.**

corresponding to a different average mass density. An acoustic wave is generated through the chamber and the ATL to enhance settling and the flocculated product is recovered in a concentrated fluid that exits from the bottom of the unit, whereas the dilute fluid exits from the top.

In acoustics, the transmission of a normal acoustic wave through an interface is a function of the impedance between the materials:

$$u_t = \frac{2Z_A}{Z_A + Z_B} u_i \tag{4}$$

The acoustic impedance of Kapton® has been estimated at 2 MRy.[26] The acoustic impedance of water is 1.6 MRy and therefore $\boldsymbol{u_t} = 0.88\boldsymbol{u_i}$. Therefore, the majority of the acoustic wave passes through the ATL, whereas for the fluid the ATL represents a no-slip barrier such as a plate used in inclined settlers.

Here, we present the performance results of laboratory-scale UEIS device used to harvest *N. oculata* and *Saccharomyces cerevisiae* cells. Polyamide particles were also used to assess the performance of the unit.

### *The acoustic harvester*

The components of the laboratory-scale UEIS unit are shown in Figure 3. The acoustic harvester consists of a set of aluminum-holding plates, driving transducer disk, driving glass plate, chamber body, acoustic transparent membrane, sensing transducer disk, and reflector glass. The lead zirconate titanate (PZT) transducer disks were obtained from Steiner & Martins (Miami, FL) made from a modified PZT-4 material. The driving disk was chosen with a resonance frequency of 1.5 MHz ± 5%. The sensing piezoelectric had a different resonance frequency of 2.5 MHz ± 100 KHz to offset the natural frequencies of the chamber and to obtain an accurate measurement of the resonance modes of the system. Both the driving and the reflector plates were made of glass

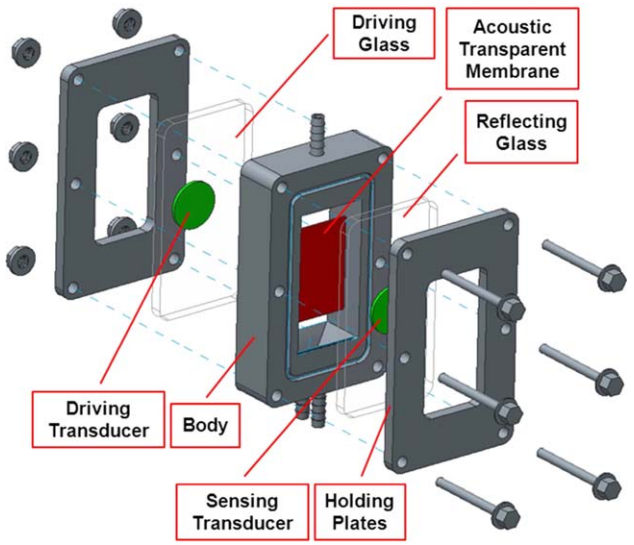


**Figure 3. Design of the UEIS device indicating the driving and sensing PZT and reflecting plates.**

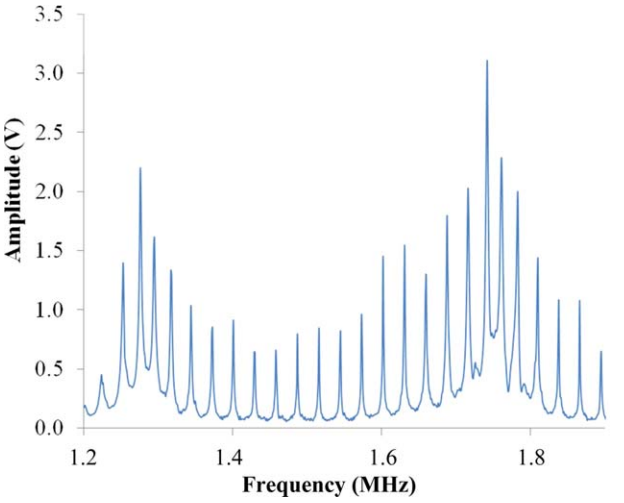


**Figure 4. Acoustic frequency response of the UEIS using a sinusoidal excitation signal of 5 $V_{pp}$ and a frequency sweep of 1 Hz increment. The water resonance modes are spaced every 29 kHz and the best resonance condition is close to 1,742 kHz.**

to enable the visual observation of the acoustic flocculation inside the chamber. The glass driving plate had 3/16″ thickness and the reflector plate was 1/4″ thick to match the acoustic resonance of the water layer in the range of 1.6–1.8 MHz as explained in the Ultrasonically Enhanced Sedimentation section. Both the driving and the sensing piezoelectric disks were attached to the glass with an epoxy bonding (liquid nails®, PPG Industries, USA). The ATL was fabricated from Kapton® polyamide film of 125 μm and a length of 2″. The chamber body was built by stereolithography using a water-resistant resin and consisted of one inlet and two outlets. The internal dimensions of the chamber were 1″ thick by 1.5″ wide by 3″ long with an internal volume of 76 mL.

### *The resonance modes*

The resonance modes of the acoustic chamber were characterized by measuring the amplitude in the frequency domain of the chamber using a driving transducer connected to a sinusoidal waveform generator (33220A, Agilent, USA), which performed a frequency sweep with a $V_{pp} = 5$ V. An opposite sensing transducer was connected to an oscilloscope (54855, Agilent Technologies, USA) that recorded amplitude and frequency. Figure 4 shows the amplitude of the transmitted acoustic signal vs. frequency. The peaks correspond to the standing waves of the chamber in which the acoustophoretic force is maximized as explained in the Ultrasonically Enhanced Sedimentation section. The largest acoustic response peak was about 1,742 kHz with adjacent modes for every 29 kHz as a consequence of the water layer thickness ($L = 1''$). This peak corresponds to a superposition of the glass reflector resonance ($f_n = 1{,}294$ kHz, 1,741 kHz, etc.) and the driving piezoelectric resonance ($f_n = 1{,}738$ kHz).

One difficulty of acoustic separation is that the resonance modes shift with the change of the temperature of the liquid layer. This phenomenon is a consequence of the variation of the speed of sound ($c$) with the temperature and has a critical impact in the acoustophoretic force and therefore the separation performance. To maintain high performance, accurate temperature control is required to combine with a frequency tracking algorithm. We designed a control algorithm in the graphical programming platform LabView® (National Instruments Corporation, USA) that performed a frequency sweep to detect the resonant modes of the chamber. A similar feedback loop has been suggested in the previous literature.[27] The amplifier was also connected to the workstation by an RS-232 cable and provided the readings of the net-amplified power supplied to the system ($P_N = P_f - P_r$).

### *Experimental setup*

The acoustic system and experimental setup is shown in Figure 5. For each set of experiments, samples of *N. oculata*, *S. cerevisiae*, or polyamide particles were placed in a graduated glass beaker and constantly mixed by a magnetic stir plate. The container was also immersed in a water bath kept at 15 ± 2°C to preserve the samples for each series of tests. This procedure also maintained the culture temperature constant and therefore the speed of sound constant to reduce the shift in the resonance frequency. The pump #1 (peristaltic pump, Masterflex L/S Digital Drive with Easy-Load II pump head, Cole-Parmer, IL) delivered the sample to the acoustic separator at the specified flow rate ($f_i$) with platinum-cured silicone tubing (Masterflex, Vernon Hills, IL). A continuous flow rate ($f_c$) was drawn from the acoustic chamber with the concentrated cell slurry by pump #2 (Masterflex C/L Variable-Speed Tubing Pump; 50–300 rpm, Cole-Parmer, Vernon Hills, IL) and returned to the sample container for its reuse after stirring. The difference between $f_i$ and $f_c$ provided the diluted flow rate ($f_d$), which returned to the sampling container for continuous agitation. The concentrated flow rate ($f_c$) was maintained constant at 1.24 mL·min$^{-1}$. All of the flow rates presented are the inlet flow rates obtained by pump #1 ($f_i$). A separate recirculating loop was used to collect the inlet sample. The sampling tubing was located next to the inlet tubing as shown in Figure 5. We obtained the samples from each returning line by collecting 3 mL of aliquots into plastic vials.

An arbitrary waveform generator was used to generate a sinusoidal wave with a peak-to-peak voltage ($V_{pp}$) of 150 mVpp that was amplified by a broadband linear RF power amplifier (350L, Electronics & Innovation, Rochester, NY)

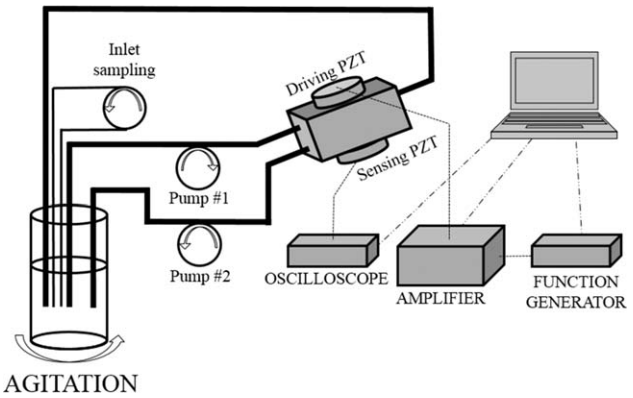


**Figure 5. Acoustic testing setup indicating the feedback recirculating loop and the PC control system.**

to generate the acoustic standing wave. The sensing piezoelectric transducer disk was connected to the digital oscilloscope that measured the frequency and amplitude of the acoustic wave. The oscilloscope and the function generator were connected to a PC workstation.

### *Sampling statistics*

The chamber residence time was calculated for each flow rate. The sample rate was defined for every two consecutive residence times. For example, for $\boldsymbol{f_i} = 25$ mL·min$^{-1}$, the residence time was 175 s. We collected three samples, one at 175 s, one at 350 s, and one at 525 s, or at each two residence times, and this was considered one test ($\boldsymbol{n} = 1$). The unit was then fully drained and rinsed. Next, the test was repeated two additional times ($\boldsymbol{n} = 3$) and the mean and standard deviation were calculated for all of the dependent variables measured. The error bars shown in Figure 5 represent the calculated standard deviations for all measurements. The inlet concentration was sampled every time to ensure a proper evaluation of the performance of the system as the sample was recirculated in each test. If the variation within the test was higher than 10%, then the test was discarded.

### *Cell cultivation, sample preparation, and acoustic contrast factor*

*N. oculata* cultures were provided by Solix Biosystems (Fort Collins, CO). The strain used was 525 from the NCMA Bigelow Laboratory for Ocean Sciences and was cultivated in a Solix AGS photobioreactor under outdoor conditions until the cell concentration reached about $3 \times 10^8$ cells·mL$^{-1}$ (dry weight, 3.2 g L$^{-1}$). The medium used was a modified *f*/2 recipe with a salinity of 16 g·L$^{-1}$, 10 mM $NO_3^-$ L$^{-1}$, 7.9 mM $PO_4^-$ L$^{-1}$, and 1 mL·L$^{-1}$ of Guillard trace metals.

*S. cerevisiae* (Brewer's yeast) and yeast extract peptone dextrose (YPD) powder were obtained from Fisher Scientific (USA). The yeast (1 g) was cultivated in 500 mL of demineralized water with 50 g·L$^{-1}$ of YPD at 27°C for 48 h until the cell concentration was $3.0 \times 10^7 \pm 9\%$ cells·mL$^{-1}$. Spherical polyamide particles (Dantec Dynamics A/S, Skovlunde, Denmark) with a mean diameter of 5 μm, $\rho = 1.05$ kg m$^{-3}$, $F = 0.05$, and $c = 2{,}200$ m s$^{-1}$ were diluted in demineralized water with surfactant Tween™ 20 at a concentration of 0.01% v/v. The concentration of the particles used was 2 g·L$^{-1}$.

The cell diameter was estimated for $\boldsymbol{n} = 25$ cells using a microscope and a measuring grid (Nikon TM-50, Japan). The mean diameter of the *N. oculata* was 3.72 μm ± 23% and for *S. cerevisiae* was 7.8 μm ± 16%. The cell density and speed of sound were measured by concentrating the cells, measuring the biovolume, and determining the speed of sound and density using an Anton Paar DSM5000 vibrating tube densitometer. The volumetric factor was computed for each sample and the cell speed of sound and density was determined using Urick's equations.[28] The results for *N. oculata* were $\rho = 1.042$ g·cm$^{-3} \pm 2\%$, $\boldsymbol{c} = 1{,}533$ m·s$^{-1} \pm 3\%$, and $\boldsymbol{F} = 0.03$ and for *S. cerevisiae* were $\rho = 1.162 \pm 1\%$, $\boldsymbol{c} = 1{,}596 \pm 2\%$, and $\boldsymbol{F} = 0.12$.

### *Cell density and separation performance*

The cell density (mL$^{-1}$) in terms of number of cells was measured using a hemocytometer counting chamber (Bright-Line, Sigma Aldrich). Ten cell counts were performed and the standard deviation was reported. The optical density was measured with a spectrophotometer at 750 nm for *N. oculata* and 600 nm for *S. cerevisiae* and polyamide particles (GENESYS™ 20, Thermo Fisher Scientific, USA) using disposable polystyrene cuvettes with a 10-mm light path (Fisherbrand™, Thermo Fisher Scientific, USA). The valid absorbance was defined between 0.1 and 1 absorbance units (Au) and all the samples were serially diluted until the absorbance was obtained in the mentioned range and the dilution factor was recorded. A calibration curve relating absorbance to cell count was derived for each sample of interest with *N. oculata* ($y = 3.7 \times 10^7 \mathrm{OD}_{750}$, $R^2 = 0.97$) *S. cerevisiae* ($y = 6.0 \times 10^6 \mathrm{OD}_{600}$, $R^2 = 0.99$) and polyamide particles ($y = 6.4 \times 10^6\ \mathrm{OD}_{600}$, $R^2 = 0.99$).

The filtration efficiency ($\varphi$) and concentration factor ($\varepsilon$) were calculated from the following equations as previously suggested in the literature[29,30]:

$$\varphi = \frac{x_\mathrm{i} - x_\mathrm{d}}{x_\mathrm{i}} \qquad \varepsilon = \frac{x_\mathrm{ctr}}{x_\mathrm{i}} \tag{5}$$

where $x_\mathrm{i}$ is the inlet cell concentration, $x_\mathrm{d}$ the diluted outlet cell concentration, and $x_\mathrm{ctr}$ the concentrated outlet cell concentration.

### *The Effects of concentration, power, flow rate, and inclination angle*

The applied Voltage ($\boldsymbol{V_{pp}}$) to the RF amplifier was varied from 50 to 300 $\mathrm{mV_{pp}}$, which corresponded to 1–13 W of net acoustic power. The forward power ($\boldsymbol{P_f}$) into the PZT and reflected power ($\boldsymbol{P_r}$) from the PZT were measured every 20 s. The net acoustic power was determined by $\boldsymbol{P_N} = \boldsymbol{P_f} - \boldsymbol{P_r}$ over the duration of the test. The standard deviation for $\boldsymbol{P_N}$ was calculated for $\boldsymbol{n} = 3$ and it is represented in the error bars.

The effect of flow rate on the filtration efficiency was determined by increasing the inlet flow rate ($\boldsymbol{f_i}$) from 20 to 80 mL·min$^{-1}$. The other variables such as $\boldsymbol{\gamma}$, $\boldsymbol{c_i}$, and $\boldsymbol{P_N}$ were kept constant for these tests. The influence of cell concentration on the separation performance was also evaluated. For these experiments, the highest culture concentration was used to determine the maximum filtration efficiency. Then, the culture was serially diluted in original media to determine the change in the performance of the unit. Finally, the effect of the inclination angle ($\gamma$) on the separation efficiency

**Table 1. Comparison with Different Designs Suggested in the Literature**

| Brief Description | Design Tested | Filtration Efficiency (%) | Concentration Factor | Settling Area ($cm^2$) |
|---|---|---|---|---|
| (a) Vertical UES harvesting chamber without internal ATL.[10,11,34] | 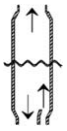 | 30 ± 7 | 3.0 ± 0.2 | 7.7 |
| (b) "U"-shaped UES harvesting with an ATL division[31] | 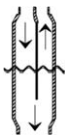 | 43 ± 7 | 3.6 ± 0.2 | 9.6 |
| (c) Inclined UES harvesting chamber without an intermediate ATL | 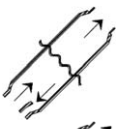 | 48 ± 6 | 2.0 ± 0.5 | 20.5 |
| (d) Inclined cell settler[33] |  | 10 ± 1 | 1.2 ± 0.1 | 34.2 |
| (e) Our design | 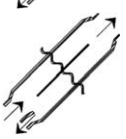 | 70 ± 5 | 11.6 ± 2.2 | 34.2 |

was determined. Specifically, the inclination of the unit was varied from 0 to 90° by using a steel protractor with a precision of ±5°.

### *Experimental comparison with other design approaches*

The filtration efficiency of the UEIS device was compared with other approaches reported in the literature for cell harvesting. We did not test competitor's devices, but we operated our device in configurations similar to those in the literature. Kilburn et al.[31] proposed several designs and one of them is the foundation for the semicontinuous acoustic separator BioSep®. This design is characterized by a vertical orientation ($\gamma = 0$) and does not use an internal ATL. One challenge of the vertical design is that the flow will create a direct opposition between the drag force and the gravity force. In this study, we tested a vertical chamber with no ATL as indicated in Table 1(a). Another design proposed by Kilburn et al. does have an internal ATL. In this design, the ATL is used to create a "U"-shaped flow in an attempt to create a settling area at the bottom of the chamber. However, a problem with this design is that the liquid bulk velocity ($v_f$) is doubled as the cross-sectional area is reduced by half. This increases the critical radius required for settling. In this study, we tested a vertical chamber with an internal ATL in a "U" configuration as indicated in Table 1(b). Another design reported in the literature uses an inclined chamber with UES.[32] Here, we tested an inclined separation chamber without intermediate ATL as indicated in Table 1(c) with $\gamma = 50°$. Another design reported in the literature uses an inclined plate settler without the use of UES.[33] Here, we tested the inclined chamber without UES and $\gamma = 50°$ as indicated in Table 1(d). To initially compare the performance of the UEIS in comparison with a similar device without UES, the UEIS device was tested as indicated in Table 1(e) with $\gamma = 50°$.

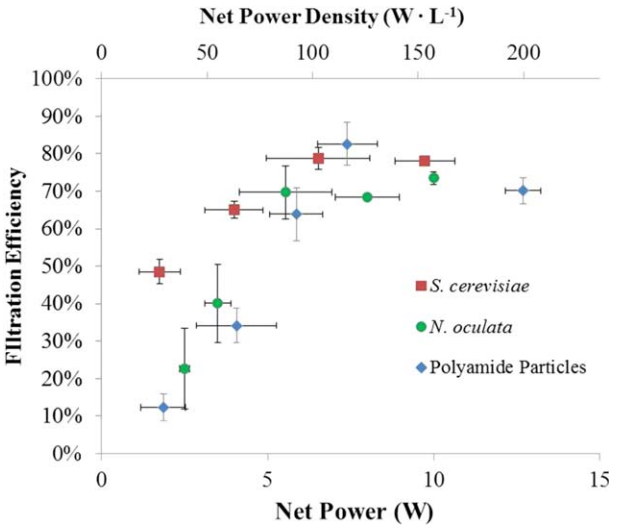


**Figure 6. Effect of the power input on the filtration efficiency with a flow rate of 25 mL·min$^{-1}$, $\gamma = 50°$, $c_i = 2.06 \times 10^9$ cells mL$^{-1}$ for *N. oculata*, $c_i = 2.03 \times 10^7$ cells mL$^{-1}$ for *S. cerevisiae*, $c_i = 2.73 \times 10^7$ cells mL$^{-1}$ for polyamide particles and $P_N = 5$ W. The filtration efficiency and the power input increased proportionally in the UEIS.**

In this study, we tested all the previously mentioned designs of Table 1 with a culture of *N. oculata* and the same conditions of cell inlet concentration ($c_i = 3.08 \times 10^8$ mL$^{-1}$), inlet flow rate ($f_i = 25$ mL min$^{-1}$), concentrated flow rate ($f_c = 1.24$ mL min$^{-1}$), and applied wave voltage ($V = 200$ mV$_{pp}$).

## Results and Discussion

### *The Effects of net input power and system throughput*

Figure 6 is a plot of filtration efficiency as a function of net power input for *N. oculata, S. cerevisiae*, and spherical polyamide particles, respectively. These experiments were conducted at a fixed inclination angle of 50°. As shown in

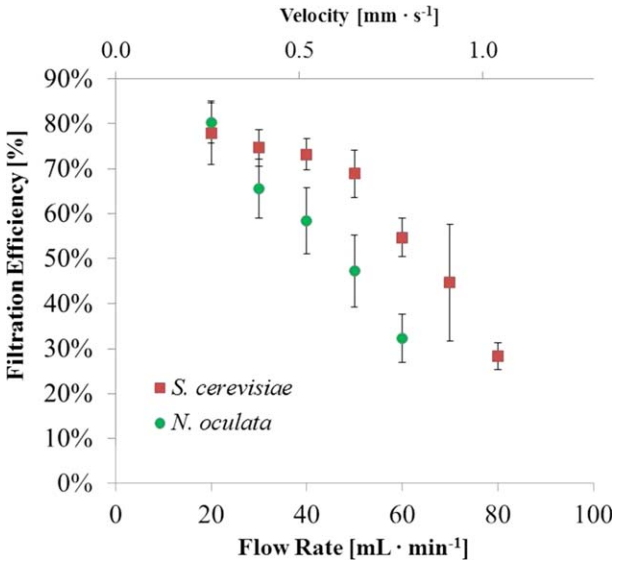


**Figure 7. The effect of flow rate and superficial fluid velocity with $c_i = 2.06 \times 10^9$ cells mL$^{-1}$ for *N. oculata*, $c_i = 2.03 \times 10^7$ cells mL$^{-1}$ for *S. cerevisiae*, $\gamma = 50°$, and a net power input $P_N = 5$ W.**

The filtration efficiency decreases with the flow rate.

Figure 6, the filtration efficiency increased with increasing net power applied to the piezoelectric disk by the amplifier for all cells and particles tested. The filtration efficiency ($\varphi$) increased sharply for the polyamide particles from $12 \pm 4\%$ at $1.9 \pm 0.7$ W to $83 \pm 6\%$ when the power was increased to $7.4 \pm 0.9$ W (equivalent to 99 W·L$^{-1}$). The similar behavior was observed for the *S. cerevisiae* culture in which an increase in filtration efficiency ($\varphi$) from $49 \pm 3$ to $79 \pm 4\%$ was observed. The efficiency also increased when the *N. oculata* cells were used. For the *N. oculata* cells, the filtration efficiency doubled when the power input was doubled. The device achieved a filtration efficiency of 70% with a net power input of 5.5 W for *N. oculata*. This corresponds to an energy consumption of 3.6 kWh·m$^{-3}$. Collectively, these results suggest a strong dependence of the filtration efficiency with $P_N$. This result is a consequence of higher acoustic power, resulting in increased acoustic energy density ($E_{ac}$) and increased acoustophoretic force acting on the particles (Eq. (1)). The increased acoustophoretic force results in increased particle velocity toward the acoustic nodes, which promotes agglomeration for enhanced settling. Nii et al. and Leong et al. also found an increasing separation efficiency with power for oil droplets and milk fat creaming.[13,35]

However, the increase in efficiency with net power was observed only for net power less than $P_N = 7.5$ W or 100 W·L$^{-1}$. At higher levels of power input, the filtration efficiency of the *S. cerevisiae* and *N. oculata* was roughly constant and the filtration efficiency for the polyamide particles decreased. We observed the presence of circulation zones in front of the driving PZT, which resulted in flow reversal that limited the performance of the unit for higher power inputs. The previous publications have suggested the formation of convective currents inside the device when the applied power is increased above a certain value.[36,37] For example, it has been shown that temperature gradients inside the chamber produce circulation patterns that inhibit particle flocculation. For this reason, some acoustic separation designs are air cooled.[38] Acoustic streaming created by the dissipation of acoustic energy has also been suggested as responsible for decreasing the separation efficiency.[39] ATLs have been used to decrease the streaming path length and enhance particle flocculation.[40]

Figure 7 is a plot of measured filtration efficiency as a function of the total system throughput (i.e. volume flow rate) and associated average bulk velocity for the *S. cerevisiae* and *N. oculata* cultures. The two samples exhibited a decrease in the filtration efficiency with increasing flow rate and liquid velocity. This result is in agreement with Eq. (3) as a higher bulk velocity results in a squared increase in the critical radii for settling. Furthermore, increasing the flow rate also decreases the residence time of the cells in the vicinity of the acoustic field, which reduces the time available for flocculation. The strongest acoustic field and therefore agglomeration was created only in front of the transducer. A new design could improve the homogeneity of the acoustic field by using larger transducers such as square or rectangular shape. Similar results of reduced performance with increasing flow rates are the characteristic of UES and inclined plate devices. Therefore, scaling up the technology will potentially require multiple units to process large flow rates with low superficial velocities. As shown in Figure 7, the reduction in filtration efficiency with increased flow rate was more dramatic for *N. oculata* in comparison to *S. cerevisiae*, which can be attributed to higher cell volume, higher density, and higher acoustic contrast factor of the yeast in comparison to the microalgae. Cells with a lower acoustic contrast factor will require more time to agglomerate in the nodes or antinodes of the acoustic field and this decreases their probability of settling for the same residence time.

### *The Effects of culture concentration and inclination angle*

As shown in Figure 8, the effect of the sample concentration on filtration efficiency was also assessed. When the sample of *S. cerevisiae* had a high cell concentration of $3.1 \times 10^7$ cells·mL$^{-1}$, the filtration efficiency was the highest at $82 \pm 4\%$ and the efficiency decreased logarithmically to $52 \pm 6\%$ when the sample was diluted to $9.25 \times 10^5$ cells·mL$^{-1}$. A similar effect was observed for the *N. oculata* cells where the highest efficiency of $75 \pm 4\%$ was achieved with a cell concentration of $3.1 \times 10^8$ cells·mL$^{-1}$ (dry weight, ca. 3.2 g L$^{-1}$) followed by an exponential decrease to $11 \pm 9\%$ at $3.1 \times 10^7$ cells·mL$^{-1}$. This decrease in the filtration efficiency can be explained by Eq. (3). Here, the acoustophoretic force is used to create a cell agglomeration larger than the critical radius of 76 μm or $1.6 \times 10^4$ cells. The agglomerated volume will settle only when the critical radius is exceeded. However, the cells can only travel $\lambda/4$ and they must do it while passing through the acoustic field. Therefore, decreasing the cell concentration will decrease the number of cells available in the $\lambda/4$ vicinity to achieve $r_c$. Also, farther cells will have to travel a longer distance to achieve $r_c$, and the probability of the agglomerated volume exiting the acoustic field before the critical radius is achieved will be higher. This logarithmic dependence with the concentration has also been reported in the previous publications.[36] The cell concentration required to exceed a filtration efficiency of 50% in our experiments was $5 \times 10^5$ cells mL$^{-1}$ for the *S. cerevisiae* and $7 \times 10^7$ cells mL$^{-1}$ for *N. oculata* cells. *N. oculata* cells require a higher cell concentration owing to their lower density, smaller cell diameter, and lower acoustic contrast factor in comparison to *S.*

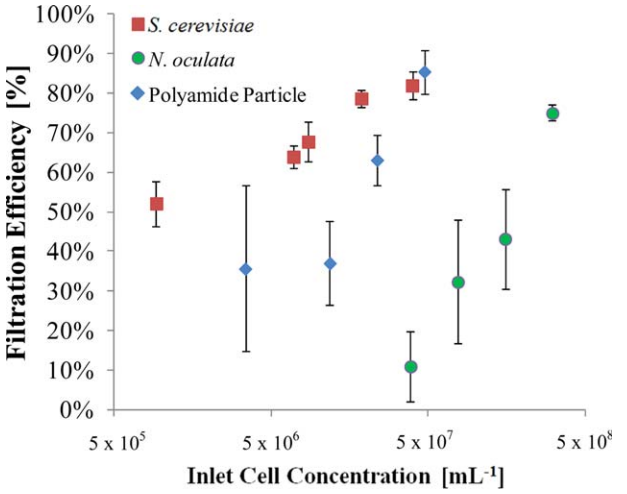


**Figure 8. The effect of cell concentration on the filtration efficiency with a flow rate of 25 mL·min$^{-1}$, $\gamma = 50°$, and a net power input $P_N = 5$ W for the UEIS.**

Lower inlet cell concentration reduces the filtration efficiency of the UEIS.

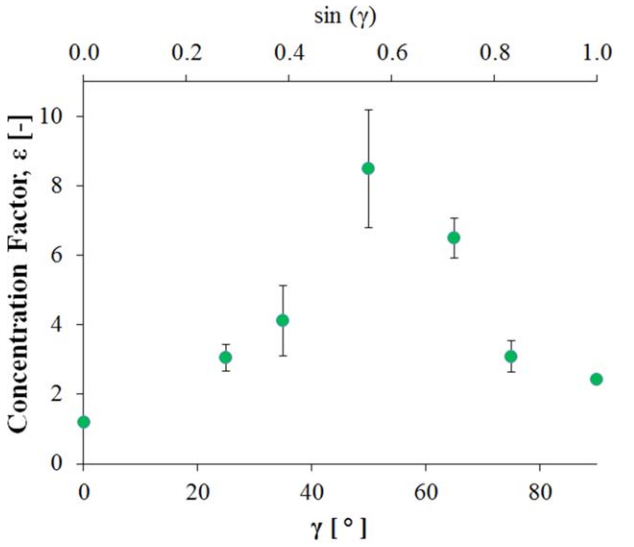


**Figure 9. The effect of the inclination angle with a flow rate of 25 mL min$^{-1}$, constant inlet cell concentration of $c_i = 2.06 \times 10^9$ cells mL$^{-1}$ for *N. oculata* and input voltage of 200 mVpp for the UEIS.**

There is an optimal angle of operation at $50 \pm 5°$.

*cerevisiae*. However, as *Nannochloropsis* sp. bioreactors usually operate in cell concentrations of $10^8$ cells mL$^{-1}$,[41] the UEIS described herein is a viable technology for this application. More work will need to be done to achieve reasonable filtration efficiencies for more dilute cultures such as those more typical in open ponds as the efficiency of the UEIS device achieved filtration efficiencies of 30% or lower under these dilute conditions of $6 \times 10^7$ cells·mL$^{-1}$.

Finally, as shown in Figure 9, the influence of the inclination angle on the concentration factor ($\varepsilon$) was assessed. The concentration factor is defined as the ratio of the outlet concentration to the inlet concentration. The results of this study suggest a very strong dependence of inclination angle ($\gamma$) on the measured concentration factor. The concentration factor increased from $1.2 \pm 0.1$ when the UEIS was operated horizontally ($\gamma = 0°$) to $8.5 \pm 1.9$ when the unit was inclined to $\gamma = 50°$. The concentration factor decreased to $2.4 \pm 0.1$ when the unit was vertically oriented ($\gamma = 90°$). The separation performance is inversely proportional to the angle. Under vertical operation, the critical radius is the largest. However, under horizontal operation, the critical radius is zero but it is difficult to recover the biomass while avoiding clogging of the unit without greatly increasing the fluid velocities owing to the constraint in cross-sectional area. The increase in the angle produces a self-cleaning effect on the inclined plates wherein the biomass slides along the inclined plates and settles at the bottom of the unit for its recovery.[42] Here, the optimum angle that results in maximum self-cleaning effect while minimizing critical settling radii was found to occur at $\gamma = 50°$. Other applications for inclined settling have reported optimum inclination angles of 50–60°.[43]

### *Comparison of the UEIS with other designs*

The results of Table 1 show that the UEIS achieved the highest filtration efficiency of $70 \pm 5\%$ and a concentration factor of $11.6 \pm 2.2$. The control inclined plate settler, which was configured as described by Thompson and Wilson[33] without UES, achieved a filtration efficiency of $10 \pm 1\%$ and a concentration factor of $1.2 \pm 0.1$. A similar configuration has been successfully used for animal cells.[24] However, as explained in the Ultrasonically Enhanced Sedimentation section, the *N. oculata* cells are smaller than those reported by Choo et al.[24] and have a density closer to that of water. This indicates that the increased gravity effect alone did not separate the microalgae cells from the continuous flow. Therefore, the use of the acoustophoretic settling resulted in a factor of 7 increase in filtration efficiency under the same conditions of velocity, angle, and cell concentration. The chamber was also oriented vertically ($\gamma = 0°$) with and without a "U" flow divider as previously suggested by Kilburn et al.[31] The results are summarized in Table 1(a) and (b). The efficiency of the vertical chamber without ATL divider was $30 \pm 7\%$ which was lower than the same configuration with the divider ($43 \pm 7\%$). This result indicates that the divider enhanced the performance of the chamber by forcing a change in the fluid direction.

Inclined plate settlers increase the effective settling area that results from the projection of the extended area in the horizontal plane. The extended settling surface area equation is defined elsewhere.[44] The calculated surface area for each configuration is given in Table 1. The effective area for cases (a) and (b) was considered as the area of the bottom outlet. Both options had similar performance with the "U"-shaped design slightly superior in terms of filtration efficiency. However, the small settling area combined with the direct opposition of the gravity and drag force in both cases results in a lower filtration efficiency compared to the UEIS. The UEIS reported herein resulted in a twofold increase in filtration efficiency and concentration factor. A benefit of the "U" design is faster biomass recovery, which could be an important criterion for sensitive cells that require low residence times inside the chamber.

The UEIS was also compared with an inclined chamber proposed elsewhere where the acoustic propagation axis has an acute angle with the flow.[32] The difference between the UEIS and this design is the presence of an inner ATL for inclined settling, and hence the effective area can be increased as summarized in Table 1(c) and (e). The UEIS had a factor of 1.5 higher filtration efficiency than the inclined chamber without ATL. This increase in the filtration

efficiency was proportional to the increase in the projected area as a consequence of the ATL.

In conclusion, the UEIS design produced 1.5- to 7.5-fold higher filtration efficiencies than other design approaches suggested in the literature when compared under the same conditions of flow rate, cell concentration, and power. Further study is required to reduce its energy consumption.

## Conclusions

Microalgae harvesting is a critical challenge for the scaleup of microalgae-derived biofuels and bioproducts. UES offers an alternative to existing methods for harvesting microalgae cells with no moving parts, suggesting lower operational and maintenance costs. Here, we presented a novel design that was developed by a combination of UES and inclined settling. A laboratory-scale UEIS was built with an internal ATL and with an effective settling area higher than other designs.

The results of this study showed that the filtration efficiency of the UEIS device decreased with increasing flow rate. The filtration efficiency increased proportionally with the input power for lower net input power but decreased after a net power input of 100 W $L^{-1}$, which could be attributed to convective currents inside the device. It was found that an optimal operational inclination angle existed at 50°. Higher inlet cell concentrations increased logarithmically the performance of the unit. The UEIS design was compared with the previous designs suggested in the literature under the same conditions of flow rate, power, and inclination, and it was found that the performance is 1.5 to 7.5 times higher in terms of the filtration efficiency. Overall, the use of UEIS design was successfully demonstrated for *N. oculata* and *S. cerevisiae*.

## Acknowledgment

The authors want to kindly thank SolixBiosystems Inc., for the *N. oculata* cultures and the NSF-IGERT 0801707 Program for providing initial funding in this research.

## Literature Cited

1. Demirbas MF. Biofuels from algae for sustainable development. *Appl Energy* 2011;88:3473–3480.
2. Chisti Y. Biodiesel from microalgae beats bioethanol. *Trends Biotechnol*. 2008;26:126–131.
3. Mata TM, Martins AA, Caetano NS. Microalgae for biodiesel production and other applications: a review. *Renew Sust Energy Rev*. 2010;14:217–232.
4. Wang B, Li YQ, Wu N, Lan CQ. CO(2) bio-mitigation using microalgae. *Appl Microbiol Biotechnol*. 2008;79:707–718.
5. Fabregas J, Herrero C. Marine microalgae as a potential source of single cell protein (SCP). *Appl Microbiol Biotechnol*. 1985; 23:110–113.
6. O'Connell D, Savelski M, Slater CS. Life cycle assessment of dewatering routes for algae derived biodiesel processes. *Clean Technol Environ Policy*. 2013;15:567–577.
7. Sander K, Murthy GS. Life cycle analysis of algae biodiesel. *Int J Life Cycle Assess*. 2010;15:704–714.
8. Uduman N, Qi Y, Danquah MK, Forde GM, Hoadley A. Dewatering of microalgal cultures: a major bottleneck to algae-based fuels. *J Renew Sust Energy*. 2010;2:15.
9. Baker NV. Segregation and sedimentation of red blood-cells in ultrasonic standing waves. *Nature*. 1972;239:398–399.
10. Gaida T, Doblhoff-Dier O, Strutzenberger K, Katinger H, Burger W, Gröschl M, Handl B, Benes E. Selective retention of viable cells in ultrasonic resonance field devices. *Biotechnol Prog*. 1996;12:73–76.
11. Ryll T, Dutina G, Reyes A, Gunson J, Krummen L, Etcheverry T. Performance of small-scale CHO perfusion cultures using an acoustic cell filtration device for cell retention: characterization of separation efficiency and impact of perfusion on product quality. *Biotechnol Bioeng*. 2000;69:440–449.
12. Dionne J, McCarthy B, Ross-Johnsrud B, Masi L, Lipkens B. Large volume flow rate acoustophoretic phase separator for oil water emulsion splitting. *Proceedings of Meetings on Acoustics*. 2013;19:045003.
13. Leong T, Johansson L, Juliano P, Mawson R, McArthur S, Manasseh R. Design parameters for the separation of fat from natural whole milk in an ultrasonic litre-scale vessel. *Ultrason Sonochem*. 2014;21:1289–1298.
14. Juliano P, Swiergon P, Mawson R, Knoerzer K, Augustin MA. Application of ultrasound for oil separation and recovery of palm oil. *J Am Oil Chem Soc*. 2013;90:579–588.
15. Kilburn DG, Clarke DJ, Coakley WT, Bardsley DW. Enhanced sedimentation of mammalian cells following acoustic aggregation. *Biotechnol Bioeng*. 1989;34:559–562.
16. Hawkes JJ, Radel S. Acoustofluidics 22: multi-wavelength resonators, applications and considerations. *Lab Chip*. 2013;13:610–627.
17. Leong T, Johansson L, Juliano P, McArthur SL, Manasseh R. Ultrasonic separation of particulate fluids in small and large scale systems: a review. *Ind Eng Chem Res*. 2013;52:16555–16576.
18. Bosma R, van Spronsen WA, Tramper J, Wijffels RH. Ultrasound, a new separation technique to harvest microalgae. *J Appl Phycol*. 2003;15:143–153.
19. Bruus H. Acoustofluidics 7: the acoustic radiation force on small particles. *Lab Chip*. 2012;12:1014–1021.
20. King LV. On the acoustic radiation pressure on spheres. *Proc R Soc Lond A*. 1934;147:212–240.
21. Lenshof A, Evander M, Laurell T, Nilsson J. Acoustofluidics 5: building microfluidic acoustic resonators. *Lab Chip*. 2012;12: 684–695.
22. Hawkes JJ, Limaye MS, Coakley WT. Filtration of bacteria and yeast by ultrasound-enhanced sedimentation. *J Appl Microbiol*. 1997;82:39–47.
23. Boycott AE. Sedimentation of blood corpuscles. *Nature*. 1920; 104:532.
24. Choo CY, Tian Y, Kim WS, Blatter E, Conary J, Brady CP. High-level production of a monoclonal antibody in murine myeloma cells by perfusion culture using a gravity settler. *Biotechnol Prog*. 2007;23:225–231.
25. Pohlscheidt M, Jacobs M, Wolf S, Thiele J, Jockwer A, Gabelsberger J, Jenzsch M, Tebbe H, Burg J. Optimizing capacity utilization by large scale 3000 L perfusion in seed train bioreactors. *Biotechnol Prog*. 2013;29:222–229.
26. Haller MI, Khuriyakub BT. 1–3 Composites for ultrasonic air transducers. *IEEE 1992 Ultrasonics Symposium: Proceedings*. 1992;1–2:937–939.
27. Hawkes JJ, Coakley WT. A continuous flow ultrasonic cell-filtering method. *Enzyme Microbial Technol*. 1996;19:57–62.
28. Urick RJ. A sound velocity method for determining the compressibility of finely divided substances. *J Appl Phys*. 1947;18: 983–987.
29. Bohm H, Briarty LG, Lowe KC, Power JB, Benes E, Davey MR. Quantification of a novel h-shaped ultrasonic resonator for separation of biomaterials under terrestrial gravity and microgravity conditions. *Biotechnol Bioeng*. 2003;82:74–85.
30. Benes E, Groschl M, Nowotny H, Trampler F, Keijzer T, Bohm H, Radel S, Gherardini L, Hawkes JJ, Konig R, Delouvroy CH. Ultrasonic separation of suspended particles. *2001 IEEE Ultrasonics Symposium Proceedings*. 2001;1–2:649–659.
31. Kilburn DG, Piret JM, Sonderhoff SA, Trampler F, Inventors. Acoustic filter for separating and recycling suspended particles. US Patent Office ##5,626,767, assignee. 1997.
32. Wang Z, Feke D, Inventors. 2011/0262990, assignee. Acoustic device and methods thereof for separation and concentration. US Patent Office Application 2011/0262990. 2011.
33. Thompson JK, Wilson JS, Inventors. Particle settler for use in cell culture. US Patent #5,817,505. 1998.
34. Doblhoffdier O, Gaida T, Katinger H, Burger W, Groschl M, Benes E. A novel ultrasonic resonance field device for the retention of animal-cells. *Biotechnol Prog*. 1994;10:428–432.

35. Nii S, Kikumoto S, Tokuyama H. Quantitative approach to ultrasonic emulsion separation. *Ultrason Sonochem.* 2009;16: 145–149.
36. Pui PWS, Trampler F, Sonderhoff SA, Groeschl M, Kilburn DG, Piret JM. Batch and semicontinuous aggregation and sedimentation of hybridoma cells by acoustic resonance fields. *Biotechnol Prog.* 1995;11:146–152.
37. Trampler F, Sonderhoff SA, Pui PWS, Kilburn DG, Piret JM. Acoustic cell filter for high-density perfusion culture of hybridoma cells. *Biotechnology.* 1994;12:281–284.
38. Shirgaonkar IZ, Lanthier S, Kamen A. Acoustic cell filter: a proven cell retention technology for perfusion of animal cell cultures. *Biotechnol Adv.* 2004;22:433–444.
39. Spengler JF, Jekel M, Christensen KT, Adrian RJ, Hawkes JJ, Coakley WT. Observation of yeast cell movement and aggregation in a small-scale MHz-ultrasonic standing wave field. *Bioseparation.* 2000;9:329–341.
40. Spengler J, Jekel M. Ultrasound conditioning of suspensions—studies of streaming influence on particle aggregation on a lab- and pilot-plant scale. *Ultrasonics.* 2000;38:624–628.
41. Richmond A, Cheng-Wu Z. Optimization of a flat plate glass reactor for mass production of Nannochloropsis sp outdoors. *J Biotechnol.* 2001;85:259–269.
42. Yao KM. Theoretical study of high-rate sedimentation. *J Water Pollut Control Fed.* 1970;42:218–228.
43. Smith BT, Davis RH. Particle concentration using inclined sedimentation via sludge accumulation and removal for algae harvesting. *Chem Eng Sci.* 2013;91:79–85.
44. Henzler HJ. Continuous fermentation with animal cells Part 2. Techniques and methods of cell retention. *Chemie Ingenieur Technik.* 2012;84:1482–1496.

Manuscript received Jun. 25, 2014, and revision received Nov. 12, 2014.